physica status solidi b

www.pss-b.com

basic solid state physics

Feature Article

Light–matter interaction in photonic crystal slabs

Lucio Claudio Andreani[1] and **Dario Gerace**[1, 2]

[1] Dipartimento di Fisica "A. Volta", Università degli Studi di Pavia, Via Bassi 6, 27100 Pavia, Italy
[2] Institute of Quantum Electronics, ETH Zurich, 8093 Zurich, Switzerland

Received 2 May 2007, revised 20 June 2007, accepted 4 July 2007
Published online 23 August 2007

PACS 42.50.Ct, 42.70.Qs, 42.82.Et, 71.35.–y, 71.36.+c, 78.20.Bh

A theoretical treatment of waveguide-embedded photonic crystals based on a guided-mode expansion method is reviewed. The following issues are discussed: (i) a formulation of the method for calculating photonic-mode dispersion and intrinsic losses due to out-of-plane diffraction, (ii) modelling of disorder-induced losses due to fabrication imperfections, and (iii) a quantum-mechanical treatment of radiation-matter interaction, with application to exciton-polaritons in photonic crystal slabs.

phys. stat. sol. (b) **244**, No. 10, 3528–3539 (2007) / **DOI** 10.1002/pssb.200743182

WILEY-VCH

phys. stat. sol. (b) **244**, No. 10, 3528–3539 (2007) / **DOI** 10.1002/pssb.200743182

Feature Article

Light–matter interaction in photonic crystal slabs

Lucio Claudio Andreani[*, 1] and **Dario Gerace**[1, 2]

[1] Dipartimento di Fisica "A. Volta", Università degli Studi di Pavia, Via Bassi 6, 27100 Pavia, Italy
[2] Institute of Quantum Electronics, ETH Zurich, 8093 Zurich, Switzerland

Received 2 May 2007, revised 20 June 2007, accepted 4 July 2007
Published online 23 August 2007

PACS 42.50.Ct, 42.70.Qs, 42.82.Et, 71.35.–y, 71.36.+c, 78.20.Bh

A theoretical treatment of waveguide-embedded photonic crystals based on a guided-mode expansion method is reviewed. The following issues are discussed: (i) a formulation of the method for calculating photonic-mode dispersion and intrinsic losses due to out-of-plane diffraction, (ii) modelling of disorder-induced losses due to fabrication imperfections, and (iii) a quantum-mechanical treatment of radiation-matter interaction, with application to exciton-polaritons in photonic crystal slabs.

1 Introduction

Photonic crystals realized in planar waveguides, commonly known as *photonic crystal slabs*, are at the heart of current interest in periodic dielectric structures thanks to their capability to control propagation of light in all spatial directions [1–4]. This is achieved by combining Bragg reflection due to a two-dimensional (2D) lattice in the slab plane with total internal reflection in the vertical direction. In particular, semiconductors are very suited for the realization of PhC slabs, due to their high refractive index yielding good confinement properties and to the availability of mature processing technologies. The lithographic definition of the 2D lattice allows introducing line and point defects, which behave as linear waveguides and nanocavities, respectively.

A crucial issue related to PhC slabs is that of losses, especially due to scattering (diffraction) out of the slab plane. Photonic modes whose dispersion lies above the cladding light line(s) in the $k - \omega$ plane are subject to intrinsic losses, as they are coupled to leaky modes of the slab, and are usually called quasi-guided. On the other hand, modes lying below the cladding light line(s) in the $k - \omega$ plane are lossless, or truly guided, in an ideal structure without disorder, and are subject only to extrinsic losses due to fabrication imperfections. Point defects in PhC slabs behave as nanocavities with full photonic confinement and their quality (Q) factor is also determined by diffraction losses, both intrinsic and extrinsic. Linear waveguides with ultra-low propagation losses have been recently achieved [5–7]. Also, spectacular progress has been achieved in demonstrating nano-cavities with extremely high Q-factors in thin Silicon [8–10] and GaAs [11] slabs. The excellent control and knowledge of photonic states in PhC slabs makes it possible to study highly interesting phenomena related to the coupling between light and matter, like optical switching [12, 13], low-threshold lasing [14], and the strong-coupling regime of radiation-matter interaction [15, 16].

In this paper we review a theoretical approach to PhC slabs in relation with the above-mentioned issues. In Section 2 we describe a Guided-Mode Expansion (GME) method for calculating photonic mode dispersion and diffraction losses in ideal (non-disordered) structures, which relies on an expansion in a

* Corresponding author: e-mail: andreani@fisicavolta.unipv.it, Phone: +39 0382 987491, Fax: +39 0382 987563

three-dimensional (3D) basis set and on the use of perturbation theory for losses. In Section 3, extension of the method to calculate disorder-induced losses is described. In Section 4 we present a quantum-mechanical formulation of radiation–matter interaction, relying on the classical calculation of photonic modes by the GME method, with application to the coupling between PhC slab modes and quantum-well excitons leading to *photonic crystal polaritons*. Section 5 contains concluding remarks. Numerical results in this paper are given for PhC slabs realized in a self-standing membrane made of a high-index material, although most of the formalism and theoretical considerations apply to more general slab structures.

2 Guided-mode expansion method

Solving Maxwell equations for a PhC slab structure is a complicated numerical task, especially for what concerns quasi-guided modes and their diffraction losses. The basic idea of the GME method is to represent the electromagnetic field in a finite basis set consisting of the guided modes of an effective homogeneous waveguide. We start from the second-order equation for the magnetic field in a source-free dielectric medium and for harmonic time dependence,

$$\nabla \times \left[\frac{1}{\varepsilon(\boldsymbol{r})} \nabla \times \boldsymbol{H} \right] = \frac{\omega^2}{c^2} \boldsymbol{H} \,. \tag{1}$$

Due to translational invariance in the slab (xy) plane implying Bloch-Floquet theorem, the magnetic field can be expanded on a basis in which planar and vertical coordinates are factorized

$$\boldsymbol{H}_{\boldsymbol{k}}(\boldsymbol{r}) = \sum_{\boldsymbol{G}} \sum_{\alpha} c_{\boldsymbol{k}+\boldsymbol{G},\alpha} \boldsymbol{h}_{\boldsymbol{k}+\boldsymbol{G},\alpha}(z)\, \mathrm{e}^{i(\boldsymbol{k}+\boldsymbol{G})\,\rho} \,, \tag{2}$$

where $\boldsymbol{r} = (\rho, z)$, $\boldsymbol{k}$ is the in-plane Bloch vector in the first Brillouin zone (BZ), $\boldsymbol{G}$ are reciprocal lattice vectors, and the functions $\boldsymbol{h}_{\boldsymbol{k}+\boldsymbol{G},\alpha}(z)$ ($\alpha = 1, 2, \ldots$) are the (discrete) guided modes of the effective planar waveguide with an average dielectric constant $\bar{\varepsilon}_j$ in each layer $j = 1, 2, 3$, calculated from the air fraction of the given photonic lattice. Thus, Eq. (1) is reduced to a linear eigenvalue problem

$$\sum_{\boldsymbol{G}'} \sum_{\alpha'} \mathcal{H}^{\alpha,\alpha'}_{\boldsymbol{k}+\boldsymbol{G},\boldsymbol{k}+\boldsymbol{G}'} c_{\boldsymbol{k}+\boldsymbol{G}',\alpha'} = \frac{\omega^2}{c^2} c_{\boldsymbol{k}+\boldsymbol{G},\alpha} \,, \tag{3}$$

where the matrix $\mathcal{H}$ is given by

$$\mathcal{H}^{\alpha,\alpha'}_{\boldsymbol{k}+\boldsymbol{G},\boldsymbol{k}+\boldsymbol{G}'} = \int \frac{1}{\varepsilon(\boldsymbol{r})} (\nabla \times \boldsymbol{h}^*_{\boldsymbol{k}+\boldsymbol{G},\alpha}(\boldsymbol{r})) \cdot (\nabla \times \boldsymbol{h}_{\boldsymbol{k}+\boldsymbol{G}',\alpha'}(\boldsymbol{r}))\, \mathrm{d}\boldsymbol{r} \,. \tag{4}$$

This formulation of the electromagnetic problem has strong analogies with the quantum-mechanical treatment of electrons, with the Hermitian matrix $\mathcal{H}$ playing the role of a Hamiltonian. The explicit expressions for the matrix $\mathcal{H}$ are given in Ref. [17] and the properties of the specific photonic lattice enter via the Fourier transform of the inverse dielectric constant in each layer, $\eta_j(\boldsymbol{G}, \boldsymbol{G}') = \varepsilon_j^{-1}(\boldsymbol{G}, \boldsymbol{G}')$, the matrix inversion being performed numerically. The eigenvalue problem (3) is solved by numerical diagonalization and the resulting photonic modes are classified according to their band index, n, and their in-plane Bloch vector $\boldsymbol{k}$. Once the magnetic field is calculated, the electric field is obtained from

$$\boldsymbol{E}_{\boldsymbol{k}}(\boldsymbol{r}) = \frac{ic}{\omega \varepsilon(\boldsymbol{r})} \nabla \times \boldsymbol{H}_{\boldsymbol{k}}(\boldsymbol{r}) \,. \tag{5}$$

The fields $\boldsymbol{E}_{kn}(\boldsymbol{r})$ and $\boldsymbol{H}_{kn}(\boldsymbol{r})$ calculated by the GME approach satisfy the orthonormality conditions

$$\int \varepsilon(\boldsymbol{r}) \boldsymbol{E}^*_{kn}(\boldsymbol{r}) \cdot \boldsymbol{E}_{k'n'}(\boldsymbol{r})\, \mathrm{d}\boldsymbol{r} = \delta_{k,k'} \delta_{n,n'} \,, \tag{6}$$

$$\int \boldsymbol{H}^*_{kn}(\boldsymbol{r}) \cdot \boldsymbol{H}_{k'n'}(\boldsymbol{r})\, \mathrm{d}\boldsymbol{r} = \delta_{k,k'} \delta_{n,n'} \,, \tag{7}$$

thus they constitute a very convenient set for the second-quantized formulation to be discussed later.

The basis set consisting of the guided modes of the effective waveguide is orthonormal, but not complete, since leaky modes are not included. Coupling to leaky modes produces a second-order shift of the mode frequency: the neglect of this effect is the main approximation of the method. A comparison with exact scattering matrix calculations indicates that the second-order shift is quite small (fractional shift usually <1%) [18], at least for the low air fractions that are usually employed. Possible choices for the average dielectric constant, convergence tests and other numerical issues are discussed in Ref. [17].

When the guided modes are folded in the first Brillouin zone, many of them fall above the light line and become quasi-guided. Indeed, first-order coupling to leaky modes at the same frequency leads to a radiative decay, which can be calculated by time-dependent perturbation theory (like in Fermi Golden Rule for quantum mechanics). The imaginary part of the squared frequency of a PhC mode with Bloch vector $\boldsymbol{k}$, whose frequency lies above the cladding light lines (or at least above one of them), is given by

$$-\mathrm{Im}\left(\frac{\omega_k^2}{c^2}\right) = \pi \sum_{\boldsymbol{G}'} \sum_{\lambda=\mathrm{TE,TM}} \sum_{j=1,3} \left|\mathcal{H}_{\boldsymbol{k},\mathrm{rad}}\right|^2 \rho_j\left(\boldsymbol{k}+\boldsymbol{G}'; \frac{\omega_k^2}{c^2}\right), \tag{8}$$

where the matrix element between a guided and a leaky PhC slab mode is

$$H_{\boldsymbol{k},\mathrm{rad}} = \int \frac{1}{\varepsilon(\boldsymbol{r})} (\nabla \times \boldsymbol{H}_{\boldsymbol{k}}^*(\boldsymbol{r})) \cdot (\nabla \times \boldsymbol{h}^{\mathrm{rad}}_{\boldsymbol{k}+\boldsymbol{G}',\lambda,j}(\boldsymbol{r}))\, \mathrm{d}\boldsymbol{r}\,, \tag{9}$$

and $\rho_j(\boldsymbol{k}+\boldsymbol{G}'; \omega_k^2/c^2)$ is the 1D photonic density of states (DOS) at fixed in-plane wave vector for radiation states that are outgoing in medium $j = 1, 3$:

$$\rho_j\left(\boldsymbol{g}; \frac{\omega^2}{c^2}\right) \equiv \int_0^\infty \frac{\mathrm{d}k_z}{2\pi}\, \delta\left(\frac{\omega^2}{c^2} - \frac{g^2+k_z^2}{\bar{\varepsilon}_j}\right) = \frac{\bar{\varepsilon}_j^{1/2} c}{4\pi} \frac{\theta\left(\omega^2 - \frac{c^2 g^2}{\bar{\varepsilon}_j}\right)}{\left(\omega^2 - \frac{c^2 g^2}{\bar{\varepsilon}_j}\right)^{1/2}}. \tag{10}$$

Notice the sum over reciprocal lattice vectors and polarizations in Eq. (8), as all diffraction processes contribute to $\mathrm{Im}\,(\omega^2/c^2)$. Equations (8)–(10) generalize the expressions given in Ref. [19] to the case of an asymmetric PhC slab and to situations in which processes with $\boldsymbol{G}' \neq 0$ contribute to diffraction losses. Once $\mathrm{Im}\,(\omega^2/c^2)$ is found, the imaginary part of frequency is easily obtained as $\mathrm{Im}\,(\omega) \simeq \mathrm{Im}\,(\omega^2)/(2\omega)$.

In the matrix elements (9), we replaced the radiative modes of the PhC slab with those of the effective waveguide. This approximation is consistent with the guided-mode expansion (2), as the set of guided + leaky modes of the effective waveguide is orthonormal and complete: guided modes are kept for the calculation of the dispersion, while leaky modes are used for the perturbative calculation of losses. Thus, no problem of mode overcounting occurs in this scheme. Again, explicit expressions for the matrix elements and convergence tests as a function of numerical parameters are given in Ref. [17].

As an example of results and comparison with other methods, we discuss propagation losses in a line-defect waveguide. We consider a W1 waveguide, i.e., a missing row of holes in the triangular lattice along the ΓK direction. Results are shown in Fig. 1 and the structure is illustrated in Fig. 1(b): the channel width w equals $w_0 \equiv \sqrt{3}a$ for a W1 waveguide, where w_0 is the period along the ΓM direction of the triangular lattice, but structures with increased channel width can also be considered. In order to treat a line defect, a supercell in the ΓM direction has to be introduced. We adopt the same parameters of Ref. [20]: membrane thickness $d = 0.6a$, dielectric constant $\varepsilon = 11.56$, hole radius $r = 0.3016a$, lattice constant $a = 430.55$ nm. We consider TE-like modes (parity $\sigma_{xy} = +1$ with respect to horizontal mirror symmetry $\hat{\sigma}_{xy}$). The dispersion of the defect modes in the gap is shown in Fig. 1(a) for the modes with $\sigma_{kz} = \pm 1$ parities with respect to vertical mirror operator $\hat{\sigma}_{kz}$, i.e., reflection symmetry with respect to a vertical plane bisecting the waveguide. The propagation loss in decibel/mm is calculated as $4.34 \times 2\,\mathrm{Im}\,(k)$, where $\mathrm{Im}\,(k) = \mathrm{Im}\,(\omega)/v_g$ is the imaginary part of the wavevector and $v_g = \mathrm{d}\omega/\mathrm{d}k$ is the mode group velocity [21]. In order to avoid finite-size effect due to the supercell along ΓM, an average of the

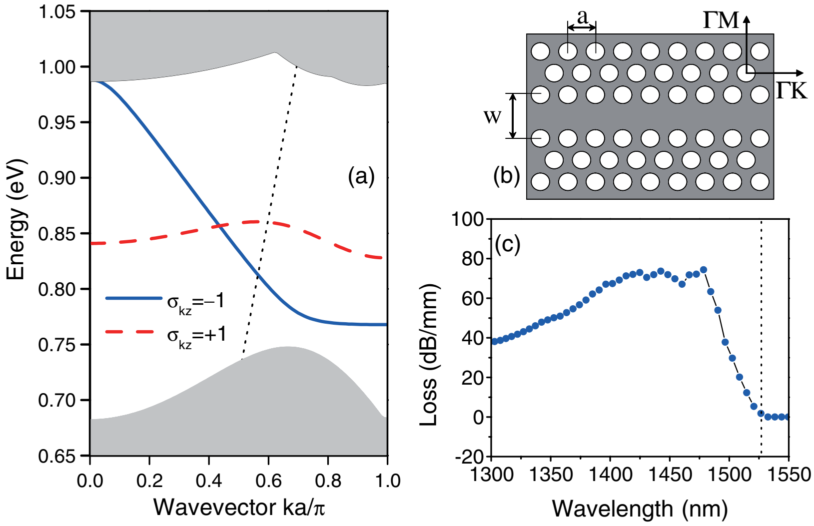

Fig. 1 (online colour at: www.pss-b.com) (a) Dispersion of the line-defect modes for a W1 waveguide structure shown in (b). The dotted line represents the light dispersion in air and the gray areas denote the photonic band regions of the 2D triangular lattice. Parameters are: self-standing membrane with thickness $d = 0.6a$, dielectric constant $\varepsilon = 11.56$, hole radius $r = 0.3016a$, lattice constant $a = 430.55$ nm. (c) Intrinsic propagation loss for the $\sigma_{kz} = -1$ mode. The dotted vertical line denotes the crossing point with the light line, where the loss goes to zero.

results over different supercell periods (typically from $3w_0$ to $10w_0$) is taken. The intrinsic propagation loss of the $\sigma_{kz} = -1$ mode is shown in Fig. 1(c) as a function of wavelength. The loss vanishes for wavelengths larger than 1527 nm, when the mode lies below the light line and is truly guided. The results of Fig. 1(c) can be compared with those reported in Fig. 2 of Ref. [20], which were calculated with the finite-difference time domain (FDTD) method [20] and previously with a Fourier modal method [22, 23]. A comparison of all results is also shown in Ref. [24]. It can be seen that the present results for propagation losses of W1 waveguide obtained with the GME method are in good agreement with those of more exact approaches. The discrepancies in the loss values are no larger than about 15% and can be attributed mainly to the approximation of replacing radiative modes of the PhC slab with those of the effective waveguide in Eq. (9).

As another example, Q-factors of nanocavity modes can be calculated within the GME method by repeating the nanocavity with a supercell in 2D and defining $Q = \omega/(2\,\mathrm{Im}\,(\omega))$. The Q-factors of L3 cavities, namely three missing rows of holes along Γ K in the triangular lattice, were shown experimentally to be larger than 45 000 in silicon membranes [8] when the local geometry is optimized by displacing the positions of the two nearby holes. The Q-factors calculated by the GME method [25] and by a Fourier modal method [26] are found to be in very good agreement with each other, reaching a maximum value of about 150 000 for a displacement $\Delta x = 0.18a$ (the Q-factor of the cavity mode for non-displaced holes is about 6 000). The strong increase of the Q-factor as a function of nearby hole displacement has been interpreted in terms of ‘gentle confinement’ of the electromagnetic field [8] as well as by matching of spatial profiles of Bloch modes that are back-reflected within the defect cavity [26]. Similarly, the Q-factor increases strongly when the nearby holes are reduced in size [25]. The combination of shifting and shrinking of the nearby holes yields a nanocavity design which is especially robust with respect to small deviations of the parameters and it has been used to enhance radiation–matter interaction in GaAs PhC membranes containing InAs quantum dots, leading to low-threshold lasing [14] and to strong coupling [16].

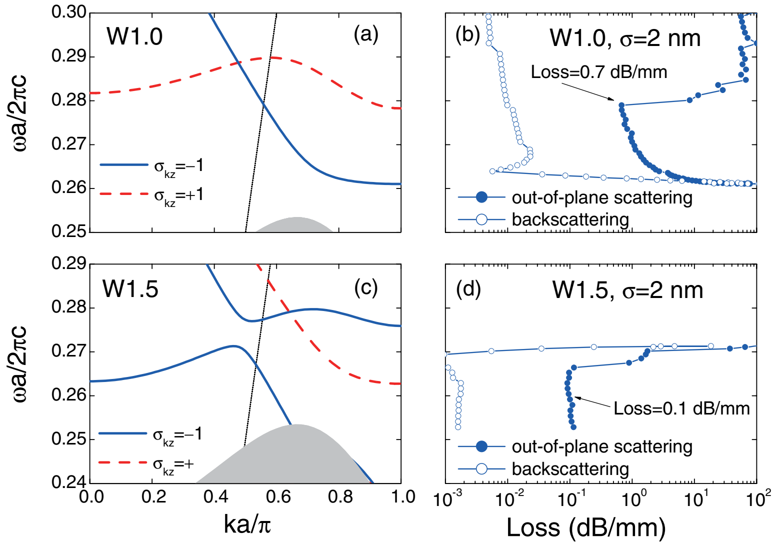

Fig. 2 (online colour at: www.pss-b.com) Dispersion and propagation losses of defect modes for W1 (a, b) and W1.5 (c, d) waveguides in a high-index membrane, assuming a slab thickness $d = 0.55a$, average hole radius $\bar{r} = 0.275a$, dielectric constant $\varepsilon = 12.11$, lattice constant $a = 420$ nm. The grey areas in (a), (c) represent the region of bulk modes.

3 Disorder-induced losses

In order to account for the effect of fabrication imperfections, we introduce a disordered lattice characterized by a spatially-dependent dielectric modulation $\varepsilon_{\text{dis}}(\boldsymbol{r})$, leading to a dielectric perturbation $\Delta\varepsilon(\boldsymbol{r}) = \varepsilon_{\text{dis}}(\boldsymbol{r}) - \varepsilon(\boldsymbol{r})$. For a given representation of disorder, the perturbation $\Delta\varepsilon(\boldsymbol{r})$ may couple truly-guided modes of the PhC slab to leaky modes, giving rise to extrinsic (disorder-induced) losses. These can be calculated again by perturbation theory, within the approximation of replacing radiative modes of the PhC slab with those of the effective waveguide. In this paper we consider a size-disorder model in which the hole radii r are randomly varied around a mean value $\bar{r}$ according to a Gaussian distribution,

$$P(r) \propto \exp\left(\frac{-(r-\bar{r})^2}{2\sigma^2}\right). \tag{11}$$

This model is characterized by a single disorder parameter, namely the r.m.s. deviation σ [27, 28]. More general two-parameter models which include micro-roughness of the hole sidewalls and allow comparison with conventional waveguides have also been studied within the present GME method [29] or with a Green function approach [30]. In order to apply the formalism outlined in Section 2, disorder is modelled within a supercell and an average over several random distributions and supercell widths is taken.

We consider a W1-type waveguide like that of Fig. 1(b), but with varying channel width w. The W1.5 waveguide, where the channel width is increased to $w = 1.5w_0$, has a single-mode region below the light line where propagation losses are expected to be very low [28, 29]: the presence of a single-mode region below the light line for both W1 and W1.5 waveguides has recently been verified experimentally [31]. Extending our previous work, we calculate also the effect of backscattering into the counter-propagating defect mode, which is described by a perturbative formula

$$-\text{Im}\left(\frac{\omega_k^2}{c^2}\right) = \pi\left|\int \frac{1}{\varepsilon_{dis}(r)}(\nabla\times\boldsymbol{H}_k^*(\boldsymbol{r}))\cdot(\nabla\times\boldsymbol{H}_{-k}(\boldsymbol{r}))\,\mathrm{d}\boldsymbol{r}\right|^2 \rho\left(-\boldsymbol{k};\frac{\omega_k^2}{c^2}\right), \tag{12}$$

where the density of states for the scattered mode at $-\boldsymbol{k}$ depends on the group velocity $v_g = \mathrm{d}\omega/\mathrm{d}k$ as

$$\rho\left(-\boldsymbol{k};\frac{\omega_k^2}{c^2}\right)=\frac{c^2}{4\pi\omega v_g}\,. \tag{13}$$

Thus the propagation loss $4.34 \times 2\ \mathrm{Im}\,(k) = 4.34 \times 2\ \mathrm{Im}\,(\omega)/v_g$ is proportional to v_g^{-2}, as first pointed out by Hughes et al. [30], and it grows rapidly in the slow-wave region where the group velocity tends to zero.

In Fig. 2(a), (c) we show the dispersion of $\sigma_{kz} = \pm 1$ line-defect modes for the W1.0 and W1.5 waveguides. A single-mode propagation region for the $\sigma_{kz} = -1$ mode (often called index-guided, or spatially even) is present in both cases. In Fig. 1(b), (d) we show the calculated propagation losses of the $\sigma_{kz} = -1$ mode, assuming a roughness parameter $\sigma = 2$ nm, for out-of-plane scattering into the leaky PhC modes (filled points) and for backscattering into the counter-propagating mode (open points). Radiation losses of the W1 waveguide become purely extrinsic and very small when the mode dispersion falls below the light line and disorder-induced scattering remains the only loss mechanism. However, they increase like $1/v_g$ in the region close to the Brillouin zone edge where v_g tends to zero. It can be seen that backscattering losses are much smaller than radiation losses in the low-loss region with high group velocity, just like in rectangular high index-contrast waveguides [32]. On the other hand, backscattering losses become dominating for the W1 waveguide close to the Brillouin-zone edge because of the $1/v_g^2$ increase [30]. Radiation losses for the W1.5 waveguide are reduced by almost one order of magnitude as compared to the standard W1 case. We notice that for the W1.5 waveguide the defect-mode dispersion below the light line has always a high group velocity, yielding a rather wide low-loss region with negligible backscattering losses.

The calculations reported in Refs. [27–29] and those shown in Fig. 2 are performed by evaluating the effect of disorder in a supercell approach in the following way: referring to Fig. 3(a), the unperturbed line-defect modes are found by solving the electromagnetic problem within the small supercell (along ΓM only), while disorder-induced modifications of the dielectric function and the resulting coupling to

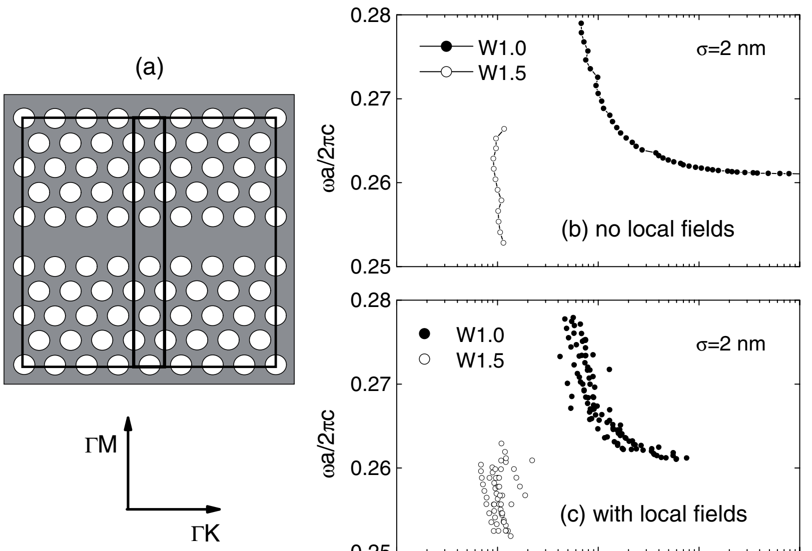

Fig. 3 (a) Scheme of a W1 waveguide, showing the small and large supercells along ΓK used in the calculations. Right: radiation losses for W1 and W1.5 waveguides in a Silicon membrane with $\varepsilon = 12.11$, slab thickness $d = 0.55a$, average hole radius $\bar{r} = 0.275a$, lattice constant $a = 420$ nm: (b) calculated without local-field effect (disorder in large supercell treated perturbatively), (c) with local-field effects (disorder in large supercell treated exactly).

leaky PhC slab modes are represented in the large supercell (along Γ M and Γ K) and are treated by perturbation theory. An average over different disorder distributions and supercell sizes is performed in order to reduce finite-size effects and to improve convergence. However, this approach does not consider changes of the local electromagnetic field due to the shifting boundaries in each hole, which require modifications of the perturbative formalism [33]. In the present guided-mode expansion based on the magnetic field, the matrix element between guided and radiation modes is expressed in terms of $\nabla \times \boldsymbol{H} = -i(\omega/c)\boldsymbol{D}$: thus the field components perpendicular to the interface (i.e., the radial components in each hole) are continuous and correctly treated, while the parallel components are not continuous and the boundary conditions for the in-plane tangential component of the field are not treated correctly.

In order to take into account the local modifications of the field due to disorder, we calculate the electromagnetic field in the large supercell of Fig. 3(a) assuming a random distribution of hole sizes and solving the problem exactly, i.e., the fields of the line-defect mode in the disordered system are obtained by solving the full eigenvalue problem without the use of perturbation theory. The eigenmodes of the fields are obtained in a folded Brillouin zone and are coupled to leaky PhC slab modes by the dielectric modulation, leading to disorder-induced propagation losses with the local-field effect being fully taken into account. An average over different disorder distributions and supercell sizes is again performed. The results of the two approaches are compared in Fig. 3(b), (c) for both W1 and W1.5 waveguides. Although the numerical spread of the results is larger in the case of the local-field calculation of Fig. 3(c), the averaged results turn out to be very close to those of the previous calculation of Fig. 3(b). Also, the ratio between the losses of W1.5 and W1 waveguides is unchanged. These results suggest that disorder-induced modifications of the local field have a minor effect on propagation losses for the present case of W1 and W1.5 waveguides. This may be due to the fact that radial field components in each hole dominate the loss behavior in the present formalism based on the magnetic field. The role of local-field effects in different structures and with other disorder models, however, is worth more detailed investigations.

4 Quantum theory of radiation–matter interaction

We consider a PhC slab with a quantum well (QW) grown in the middle of the core layer, as illustrated in Fig. 4(a). The ground-state QW exciton is usually a heavy-hole exciton, with in-plane polarization of the transition dipole, and is able to interact with TE-like ($\sigma_{xy} = +1$, even) modes of the PhC slab. In the following we take the specific case of a square lattice of holes with lattice constant a, whose photonic bands for TE-like modes are plotted in Fig. 4(b) in dimensionless units. When the QW exciton is resonant with truly-guided photonic modes below the light line (e.g., at the frequencies indicated by the two

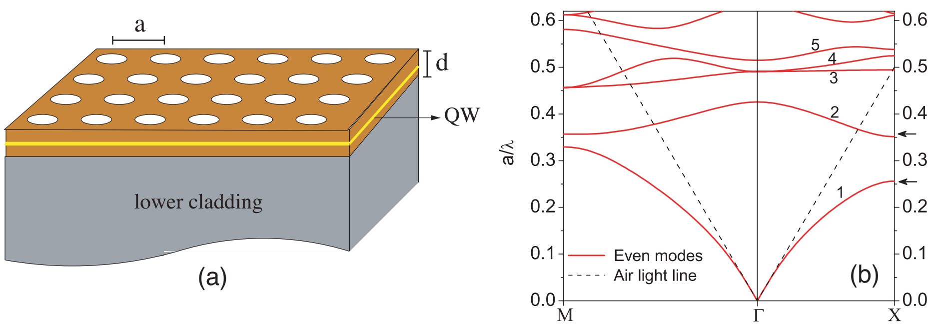

Fig. 4 (online colour at: www.pss-b.com) (a) Schematic view of a 2D photonic crystal slab with core thickness d and lattice constant a, with an embedded single quantum well at the midplane of the core layer. (b) Photonic mode dispersion (even modes, $\sigma_{xy} = +1$) for a square lattice in a high-index ($\varepsilon = 11.76$) photonic crystal membrane with $d/a = 0.3$, $r/a = 0.34$. The first few modes are labelled by a band number. Dashed lines represent the light dispersion in air.

arrows in Fig. 4(b)) it forms stationary modes which we call *guided photonic crystal polaritons*. On the other hand, when the exciton is resonant with quasi-guided photonic modes above the light line, the exciton–photon interaction can be in a weak or in a strong-coupling regime: when the exciton–photon coupling is larger than the intrinsic photonic mode linewidth, exciton-polariton states are formed, which we name *radiative photonic crystal polaritons*. Those states are especially interesting, since they can be probed by incident light from the surface of the sample in a reflectance or transmission experiment. Indeed, strong exciton–light coupling has been reported in photonic crystal slabs filled with organic excitons [34] and the semiclassical theory of the optical response has been developed using a scattering-matrix formalism, where the excitonic resonance is treated by a Lorentz oscillator [35].

Here we formulate a theory of radiation–matter interaction, which is based on a full quantization of the exciton and photon fields. In a non-homogeneous dielectric medium, the vector potential can be chosen to satisfy the generalized Coulomb gauge $\nabla \cdot (\varepsilon(\boldsymbol{r})\boldsymbol{A}(\boldsymbol{r}, t)) = 0$ and it is expanded in normal modes as

$$\hat{A}(\boldsymbol{r}, t) = \sum_{\boldsymbol{k},n} (2\pi\hbar\omega_{\boldsymbol{k}n})^{1/2} \left[\hat{a}_{\boldsymbol{k}n}\boldsymbol{A}_{\boldsymbol{k}n}(\boldsymbol{r})\,\mathrm{e}^{-i\omega_{\boldsymbol{k}n}t} + \hat{a}^{\dagger}_{\boldsymbol{k}n}\boldsymbol{A}^{*}_{\boldsymbol{k}n}(\boldsymbol{r})\,\mathrm{e}^{i\omega_{\boldsymbol{k}n}t}\right], \tag{14}$$

where $\hat{a}^{\dagger}_{\boldsymbol{k}n}$ ($\hat{a}_{\boldsymbol{k}n}$) are creation (destruction) operators of field quanta with eigenfrequencies $\omega_{\boldsymbol{k}n}$, and the indices $\boldsymbol{k}$, n are the in-plane Bloch vector and band number of each eigenmode. In order to satisfy Bose commutation relations for $\hat{a}_{\boldsymbol{k}n}$, $\hat{a}^{\dagger}_{\boldsymbol{k}n}$, the normalization conditions for the classical functions $\boldsymbol{A}_{\boldsymbol{k}n}(\boldsymbol{r})$ are

$$\int \varepsilon(\boldsymbol{r})\, \boldsymbol{A}^{*}_{\boldsymbol{k}n}(\boldsymbol{r}) \cdot \boldsymbol{A}_{\boldsymbol{k}'n'}(\boldsymbol{r})\,\mathrm{d}\boldsymbol{r} = \frac{c^2}{\omega^2_{\boldsymbol{k}n}}\,\delta_{\boldsymbol{k},\boldsymbol{k}'}\delta_{n,n'}\,, \tag{15}$$

which are equivalent to (6) and (7) for the electric and magnetic fields. Thus, the classical fields calculated by the GME method (neglecting the QW dielectric discontinuity and prior to including the exciton contribution) can be conveniently used as normal modes for second quantization. The exciton field can also be quantized by introducing operators $\hat{b}^{\dagger}_{\boldsymbol{k}\nu}$ and $\hat{b}_{\boldsymbol{k}\nu}$, which satisfy Bose commutation relations in the limit of weak excitation, using quantum number $\boldsymbol{k}$, ν analogous to those of the photon modes. Indeed, the free motion of the exciton center-of-mass in the QW plane is restricted to the dielectric region and it can be described by a 2D Schrödinger equation for the envelope function in an effective potential $V(\boldsymbol{R}_{\|})$:

$$\left[-\frac{\hbar^2\nabla^2}{2M_{\mathrm{ex}}} + V(\boldsymbol{R}_{\|})\right] F_{\boldsymbol{k}}(\boldsymbol{R}_{\|}) = E_{\boldsymbol{k}}F_{\boldsymbol{k}}(\boldsymbol{R}_{\|})\,, \tag{16}$$

where $M_{\mathrm{ex}} = m^*_{\mathrm{e}} + m^*_{\mathrm{h}}$ is the total exciton mass and the potential $V(\boldsymbol{R}_{\|}) = 0$ in the dielectric regions, while $V(\boldsymbol{R}_{\|})$ takes a large value V_{∞} in the air holes. Equation (16) can be solved by plane-wave expansion, using the same Fourier components as for the photonic modes in the slab, leading to exciton energies $E^{(\mathrm{ex})}_{\boldsymbol{k}\nu} = E_{\mathrm{ex}} + E_{\boldsymbol{k}\nu}$, where E_{ex} is the bare QW exciton energy and $E_{\boldsymbol{k}\nu}$ is the center-of-mass quantization energy in the in-plane potential $V(\boldsymbol{R}_{\|})$. Since the photonic and excitonic problems are characterized by the same 2D Bravais lattice, their interaction conserves the 2D Bloch vector $\boldsymbol{k}$. The exciton–photon Hamiltonian can be derived by second-quantizing the classical minimal-coupling hamiltonian with the $\boldsymbol{A} \cdot \boldsymbol{p}$ and $\boldsymbol{A}^2$ interaction terms. The resulting quantum Hamiltonian takes the form

$$\begin{aligned}\hat{H} = &\sum_{\boldsymbol{k},n} \hbar\omega_{\boldsymbol{k}n}\left(\hat{a}^{\dagger}_{\boldsymbol{k}n}\hat{a}_{\boldsymbol{k}n} + \frac{1}{2}\right) + \sum_{\boldsymbol{k},\nu} E^{(ex)}_{\boldsymbol{k}\nu}\hat{b}^{\dagger}_{\boldsymbol{k}\nu}\hat{b}_{\boldsymbol{k}\nu} + i\sum_{\boldsymbol{k},n,\nu} C_{\boldsymbol{k}n\nu}(\hat{a}_{\boldsymbol{k}n} + \hat{a}^{\dagger}_{-\boldsymbol{k}n})(\hat{b}_{-\boldsymbol{k}\nu} - \hat{b}^{\dagger}_{\boldsymbol{k}\nu})\\ &+ \sum_{\boldsymbol{k},\nu,n,n'} D_{\boldsymbol{k}\nu nn'}(\hat{a}_{-\boldsymbol{k}n} + \hat{a}^{\dagger}_{\boldsymbol{k}n})(\hat{a}_{\boldsymbol{k}n'} + \hat{a}^{\dagger}_{-\boldsymbol{k}n'})\,,\end{aligned} \tag{17}$$

with the coupling coefficients being given by

$$C_{\boldsymbol{k}n\nu} = E^{(\mathrm{ex})}_{\boldsymbol{k}\nu}\left(\frac{2\pi e^2\hbar\omega_{\boldsymbol{k}n}}{\hbar^2c^2}\right)^{1/2} \langle\Psi^{(\mathrm{ex})}_{\boldsymbol{k}\nu}|\sum_j \boldsymbol{A}_{\boldsymbol{k}n}(\boldsymbol{r}_j)\cdot\boldsymbol{r}_j|0\rangle\,, \tag{18}$$

physica status solidi b

while $D_{kvnn'} = C^*_{knv} C_{kn'v} / E^{(\mathrm{ex})}_{kv}$. Equation (17) has the same structure of the well-known Hopfield Hamiltonian for bulk exciton-polaritons [36, 37], however the interaction takes place between photons and excitons with the same Bloch vector $\boldsymbol{k}$ but with all pairs of quantum numbers n, v. The coefficients C_{knv} can be expressed in terms of the oscillator strength per unit area of the QW exciton, f/S, and of the overlap integral between electric field and exciton center-of-mass wavefunction in the 2D plane as

$$C_{knv} \simeq -i \left(\frac{\pi \hbar^2 e^2}{m_0} \frac{f}{S} \right)^{1/2} \int \hat{\boldsymbol{e}} \cdot \boldsymbol{E}_{kn}(\rho, z_{\mathrm{QW}})\, F^*_{kv}(\rho)\, \mathrm{d}\rho \,. \tag{19}$$

Thus, all parameters of the quantum Hamiltonian are determined from a classical calculation of the electric field eigenmodes, through the GME method outlined in Section 2, and of the exciton envelope function confined in the dielectric regions. The Hamiltonian (17) can be diagonalized by a generalized Hopfield transformation, which leads to a non-hermitian eigenvalue problem of dimension $2(N_{\max} + M_{\max}) \times 2(N_{\max} + M_{\max})$ at each bloch vector $\boldsymbol{k}$, where $N_{\max}$ and $M_{\max}$ are the number of photon and exciton modes kept in the expansion, respectively. Numerical solution of this eigenvalue problem yields finally the eigenfrequencies of the mixed exciton–photon modes. It should be noted that the dampings of photon and exciton states can be taken into account in the formalism by means of an imaginary part of their frequencies in the diagonal terms of Eq. (17). In particular, the intrinsic photon linewidth plays a crucial role in the theory: even if the exciton linewidth is assumed to be small (which requires very high-quality samples at low temperature), and for an ideal sample without disorder, quasi-guided PhC slab modes have an intrinsic linewidth arising from out-of-plane diffraction. Thus, the occurrence of radiative PhC polaritons depends on the relative size of the exciton-photon interaction (quantified by the coupling coefficients C_{knv}) versus the photonic mode linewidth Im (ω_{kn}), which is also calculated by the GME method.

We notice that a strong-coupling regime may also occur when quantum dots are embedded in PhC nanocavities [15, 16], however in that case the quantum Hamiltonian is different since quantum dot excitations are described by pseudo-spin (instead of bosonic) operators [40, 41]. Theoretical treatments of strong coupling of quantum dots in PhC slab nanocavities can be found in [42, 43]. In particular, we have shown [43] that for typical oscillator strengths of self-assembled InAs quantum dots ($f \sim 11$, corresponding to a dipole moment $d = 5.6\,|e| \cdot \text{Å} = 27$ debye) strong coupling occurs for Q-factors larger than about 2 000.

We now give examples of calculated dispersion for guided and radiative polaritons, assuming an oscillator strength per unit surface $f/S = 4 \times 10^{12}\ \mathrm{cm}^{-2}$ typical of a $\mathrm{In}_x\mathrm{Ga}_{1-x}\mathrm{As/GaAs}$ QW [44]. In Fig. 5(a) and (b) we consider the interaction of a QW exciton with photonic modes 1 and 2, respectively, from the band dispersion shown in Fig. 4(b). The lattice constant is chosen in order to have the resonance condition close to the BZ edge along the Γ X direction, for $k_x \simeq 0.95\pi/a$ [see also arrows in Fig. 4(b)]. As it can be seen from Fig. 5, the dispersion of bare exciton and photon modes is strongly modified in both cases,

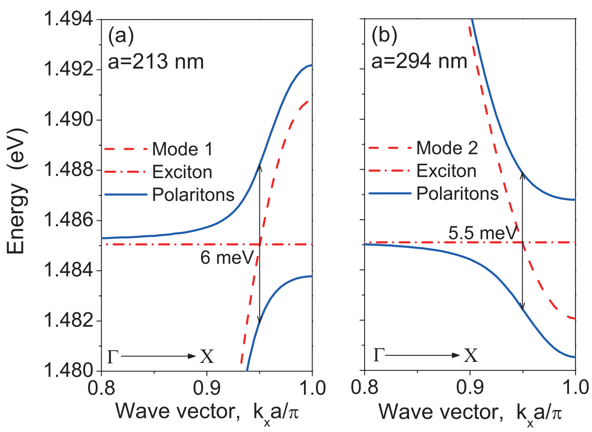

Fig. 5 (online colour at: www.pss-b.com) Guided polariton dispersion along Γ X for a photonic mode interacting with a QW exciton at $E_{\mathrm{ex}} = 1.485$eV, with oscillator strength $f/S = 4 \times 10^{12}\ \mathrm{cm}^{-2}$; the uncoupled mode dispersions are shown with dashed and dot-dashed lines, respectively. Parameters of the photonic structure are: $\varepsilon = 11.76$, $r/a = 0.34$, $d/a = 0.3$. Panel (a): coupling to the first photonic mode, lattice constant $a = 213$ nm. Panel (b): coupling to the second mode, $a = 294$ nm.

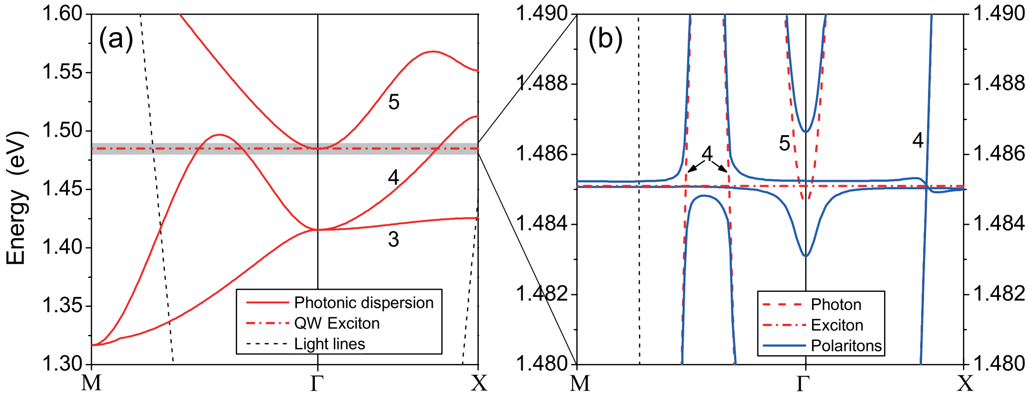

Fig. 6 (online colour at: www.pss-b.com) (a) Photonic mode dispersion around the QW exciton energy, $E_{ex} = 1.485$ eV, for structure parameters: $r/a = 0.34$, $d/a = 0.3$, $a = 430$ nm. (b) Close-up for the 10 meV energy range of interest, showing the solution for the coupled exciton–photon system (full line) together with the bare exciton and photon dispersions (dashed).

giving rise to sizable anticrossings. The strongly coupled polaritonic dispersion is compared to the bare exciton and photon dispersions (the uncoupled exciton center-of-mass levels are not shown, for simplicity). The calculated vacuum Rabi splitting is $\hbar\Omega_R = 6$ meV for the first mode and $\hbar\Omega_R = 5.5$ meV for the second one, respectively. The exciton-photon coupling is dependent on the specific band of interest, due to the different spatial profile of the corresponding electric field and thus to the modified overlap with the exciton center-of-mass wavefunctions. In any case, we point out that such values obtained with a *single* quantum well are comparable to those commonly achieved for MC polaritons with *six* QWs [38]. This arises from the increased exciton–photon coupling of Eq. (19), due to better confinement in the vertical direction of a high-index dielectric slab compared to a MC with low-index contrast distributed Bragg reflectors.

We show in Fig. 6 the case of a PhC slab of lattice constant $a = 430$ nm, in which the exciton is resonant with different photonic modes within the first BZ (those labelled with indices 4 and 5 in Fig. 4(b)). In Fig. 6(a), the bare photonic mode dispersion around $E_{ex} = 1.485$ eV is shown. It is interesting to notice the existence of a band minimum for mode 5 at the Γ-point: such feature leads to a quasi-particle dispersion similar to MC polaritons, as it will be clear in the following. Actually, the resonance condition occurs simultaneously with different modes along Γ M and Γ X. In Fig. 6(b), the dispersion of the exciton–photon coupled modes is shown in a restricted energy range around the exciton resonance. Notice that there are five resonant points between QW excitons and PhC slab modes, leading to a variety of situations for the coupled modes. Along Γ M, anticrossings can be seen with photonic modes 4 and 5, which are fingerprints of the strong coupling regime. In this case, the intrinsic radiative linewidth of bare photonic states is lower than the exciton–photon coupling energy. As the QW exciton is resonant with mode 4 for two different wave vectors along Γ M, we observe two anticrossings above the light line in the middle of the BZ. This peculiar effect is due to the light dispersion engineering allowed in PhC structures. Along Γ X, resonance with mode 5 gives strong coupling, while resonance with mode 4 at larger in-plane wave vector gives a crossing of the bare excitonic and photonic dispersions, meaning that the system is in weak coupling.

Radiative PhC polaritons can be probed by angle-resolved reflectance from the sample surface, as first done on 1D photonic crystals filled with organic molecules [34]. The same kind of experiment could be performed with semiconductor-based systems discussed in this work. Indeed, the present quantum-mechanical treatment of interacting photon and exciton states has been compared with semiclassical calculations of the surface reflectance, showing a very good agreement for the splitting in strong coupling regime [25, 39, 43]. For guided polaritons, on the other hand, coupling to an external propagating beam is prohibited due to the evanescent character of the electromagnetic field in the claddings. As shown in Fig. 6(b), a peculiar property of the square lattice is that radiative polaritons can form with an energy minimum at the Γ-point. This is similar to the dispersion of microcavity polaritons [45–48], which has usually a minimum at $\boldsymbol{k} = 0$, and which has been used in the last few years to demonstrate a number of outstanding phenomena related to parametric scattering of cavity polaritons [49, 50] and to their Bose condensation [51].

5 Conclusions

The guided-mode expansion method is seen to be a useful approach for describing photonic modes in PhC slabs, especially for calculating the dispersion and losses of quasi-guided modes as well as cavity Q-factors. The method can be generalized to calculate scattering losses of truly guided modes induced by disorder. Furthermore, the classical fields obtained by the GME method are conveniently normalized and can be used as a set of normal modes for second quantization of the electromagnetic field in a PhC slab. A quantum-mechanical theory of the interaction between photons and QW excitons has been developed and it leads to the description of photonic crystal polaritons, which can either guided or radiative. In particular, the dispersion of radiative PhC polaritons may have a minimum at $\boldsymbol{k} = 0$, in analogy to micro-cavity polaritons: this suggests the possibility of achieving polariton parametric processes in a PhC slab. In general, quantum electrodynamical processes related to light-matter interaction in PhC slabs are likely to be one of the major themes of nanophotonics in the next few years.

Acknowledgements We are grateful to M. Agio and M. Liscidini for fruitful collaboration and participation to related aspects of this research. This work was supported by MIUR through Cofin and FIRB programs, as well as by CARIPLO foundation.

References

[1] K. Sakoda, Optical Properties of Photonic Crystals (Springer, Berlin, 2001).
[2] S. G. Johnson and J. D. Joannopoulos, Photonic Crystals: The Road from Theory to Practice (Kluwer Academic Publishers, Boston, 2002).
[3] K. Busch, S. Lölkes, R. B. Wehrspohn, and H. Föll (eds.), Photonic Crystals: Advances in Design, Fabrication, and Characterization (Wiley-VCH, Weinheim, 2004).
[4] J.-M. Lourtioz, H. Benisty, V. Berger, J.-M. Gérard, D. Maystre, and A. Tchelnokov (eds.), Photonic Crystals: Towards Nanoscale Photonic Devices (Springer-Verlag, Berlin, 2005).
[5] E. Dulkeith, S. J. McNab, and Yu. A. Vlasov, Phys. Rev. B **72**, 115102 (2005).
[6] E. Kuramochi, M. Notomi, S. Hughes, A. Shinya, T. Watanabe, and L. Ramunno, Phys. Rev. B **72**, 161318(R) (2005).
[7] L. O'Faolain, X. Yuan, D. McIntyre, S. Thoms, H. Chong, R. M. De La Rue, and T. F. Krauss, Electron. Lett. **42**, 1454 (2006).
[8] T. Akahane, T. Asano, B.-S. Song, and S. Noda, Nature **425**, 944 (2003).
[9] M. Notomi, A. Shinya, S. Mitsugi, E. Kuramochi, and H.-Y. Ryu, Opt. Express **12**, 1551 (2004).
[10] B.-S. Song, S. Noda, T. Asano, and Y. Akahane, Nature Mater. **4**, 207 (2005).
[11] E. Weidner, S. Combrié, N. V. Q. Tran, A. De Rossi, J. Nagle, S. Cassette, A. Talneau, and H. Benisty, Appl. Phys. Lett. **89**, 221104 (2006).
[12] M. Notomi, A. Shinya, S. Mitsugi, G. Kira, E. Kuramochi, and T. Tanabe, Opt. Express **13**, 2678 (2005).
[13] T. Tanabe, M. Notomi, S. Mitsugi, A. Shinya, and E. Kuramochi, Appl. Phys. Lett. **87**, 151112 (2005).
[14] S. Strauf, K. Hennessy, M. T. Rakher, Y.-S. Choi, A. Badolato, L. C. Andreani, E. L. Hu, P. M. Petroff, and D. Bouwmeester, Phys. Rev. Lett. **96**, 127404 (2006).
[15] T. Yoshie, A. Scherer, J. Hendrickson, G. Khitrova, H. M. Gibbs, G. Rupper, C. Ell, O. B. Shchekin, and D. G. Deppe, Nature **432**, 2002 (2004).
[16] K. Hennessy, A. Badolato, M. Winger, D. Gerace, M. Atatüre, S. Gulde, S. Fält, E. L. Hu, and A. Imamoğlu, Nature **445**, 896 (2007).
[17] L. C. Andreani and D. Gerace, Phys. Rev. B **73**, 235114 (2006).
[18] L. C. Andreani and M. Agio, IEEE J. Quantum Electron. **38**, 891 (2002).

[19] T. Ochiai and K. Sakoda, Phys. Rev. B **64**, 045108 (2001).
[20] M. J. Cryan, D. C. L. Wong, I. J. Craddock, S. Yu, J. Rorison, and C. J. Railton, IEEE Photonics Technol. Lett. **17**, 58 (2005).
[21] L. C. Andreani and M. Agio, Appl. Phys. Lett. **82**, 2011 (2003).
[22] P. Lalanne, IEEE J. Quantum Electron. **38**, 800 (2002).
[23] C. Sauvan, P. Lalanne, J.-C. Rodier, J.-P. Hugonin, and A. Talneau, IEEE Photonics Technol. Lett. **15**, 1243 (2003).
[24] C. Sauvan, PhD thesis, Université Paris XI – Orsay (2005).
[25] L. C. Andreani, D. Gerace, and M. Agio, Photonics Nanostruct. Fundam. Appl. **2**, 103 (2004).
[26] C. Sauvan, P. Lalanne, and J.-P. Hugonin, Phys. Rev. B **71**, 165118 (2005).
[27] D. Gerace and L. C. Andreani, Opt. Lett. **29**, 1897 (2004).
[28] D. Gerace and L. C. Andreani, Opt. Express **13**, 4939 (2005).
[29] D. Gerace and L. C. Andreani, Photonics Nanostruct. Fundam. Appl. **3**, 120 (2005).
[30] S. Hughes, L. Ramunno, J. F. Young, and J. E. Sipe, Phys. Rev. Lett. **94**, 033903 (2005).
[31] M. Galli, D. Bajoni, M. Patrini, G. Guizzetti, D. Gerace, L. C. Andreani, M. Belotti, and Y. Chen, Phys. Rev. B **72**, 125322 (2005).
[32] C. G. Poulton, C. Koos, M. Fujii, A. Pfrang, T. Schimmel, J. Leuthold, and W. Freude, IEEE J. Sel. Top. Quantum Electron. **12**, 1306 (2006).
[33] S. G. Johnson, M. L. Povinelli, M. Soljacić, A. Karalis, S. Jacobs, and J. D. Joannopoulos, Appl. Phys. B **81**, 283 (2005).
[34] T. Fujita, Y. Sato, T. Kuitani, and T. Ishihara, Phys. Rev. B **57**, 12428 (1998).
[35] A. L. Yablonskii, E. A. Muljarov, N. A. Gippius, S. G. Tikhodeev, T. Fujita, and T. Ishihara, J. Phys. Soc. Jpn. **70**, 1137 (2001).
[36] J. J. Hopfield, Phys. Rev. **112**, 1555 (1958).
[37] V. M. Agranovich, Zh. Eksp. Teor. Fiz. **37**, 430 (1959) [Sov. Phys. JETP **37**, 307 (1960)].
[38] R. Houdré, C. Weisbuch, R. P. Stanley, U. Oesterle, P. Pellandini, and M. Ilegems, Phys. Rev. Lett. **73**, 2043 (1994).
[39] D. Gerace, M. Agio, and L. C. Andreani, phys. stat. sol. (c) **1**, 446 (2004).
[40] L. C. Andreani, G. Panzarini, and J.-M. Gérard, Phys. Rev. B **60**, 13276 (1999).
[41] L. C. Andreani, in: Electron and Photon Confinement in Semiconductor Nanostructures, edited by B. Deveaud, A. Quattropani, and P. Schwendimann (IOS Press, Amsterdam, 2003), p. 105.
[42] S. Hughes and H. Kamada, Phys. Rev. B **70**, 195313 (2004).
S. Hughes, Opt. Lett. **30**, 1393 (2005).
[43] D. Gerace and L. C. Andreani, phys. stat. sol. (c) **2**, 801 (2005).
L. C. Andreani, D. Gerace, and M. Agio, phys. stat. sol. (b) **242**, 2197 (2005).
[44] R. C. Iotti and L. C. Andreani, Phys. Rev. B **56**, 3922 (1997).
[45] C. Weisbuch, M. Nishioka, A. Ishikawa, and Y. Arakawa, Phys. Rev. Lett. **69**, 3314 (1992).
[46] M. S. Skolnick, T. A. Fisher, and D. M. Whittaker, Semicond. Sci. Technol. **13**, 645 (1998).
[47] K. Khitrova, H. M. Gibbs, F. Jahnke, M. Kira, and S. W. Koch, Rev. Mod. Phys. **71**, 1591 (1999).
[48] A. Kavokin and G. Malpuech, Cavity Polaritons (Elsevier, Amsterdam, 2003).
[49] P. G. Savvidis, J. J. Baumberg, R. M. Stevenson, M. S. Skolnick, D. M. Whittaker, and J. S. Roberts, Phys. Rev. Lett. **84**, 1547 (2000).
[50] M. Saba, C. Ciuti, J. Bloch, V. Thierry-Mieg, R. André, Le Si Dang, S. Kundermann, A. Mura, G. Bongiovanni, J. L. Staehli, and B. Deveaud, Nature **414**, 731 (2001).
[51] J. Kasprzak, M. Richard, S. Kundermann, A. Baas, P. Jeambrun, J. M. J. Keeling, F. M. Marchetti, M. H. Szymańska, R. André, J. L. Staehli, V. Savona, P. B. Littlewood, B. Deveaud, and Le Si Dang, Nature **443**, 409 (2006).

